

Spectral study on the dips of Cir X-1

Ya-Juan Lei¹*, Fang-Jun Lu¹, Jin-Lu Qu¹, Li-Ming Song¹ and
Cheng-Min Zhang²

¹ Laboratory for Particle Astrophysics, Institute of High Energy Physics,
Chinese Academy of Sciences, Beijing, 100049, China

² National Astronomical Observatories, Chinese Academy of Sciences, Beijing
100012, China

Abstract We present X-ray spectral analyses of low mass X-ray binary Cir X-1 during X-ray dips, using the *Rossi X-ray Timing Explorer (RXTE)* data. Each dip was divided into several segments, and the spectrum of each segment was fitted with a three-component blackbody model, in which two components are affected by partial covering and the third one is unaffected. A Gaussian emission line is also included in the spectral model to represent the Fe K α line at ~ 6.4 keV. The fitted temperatures of the two partially covered components are about 2 keV and 1 keV, while the uncovered component has a temperature of ~ 0.5 – 0.6 keV. The equivalent blackbody emission radius of the hottest component is the smallest and that of the coolest component is the biggest. During dips, the fluxes of the two hot components are linearly correlated, while that of the third component doesn't show any significant variation. The Fe line flux remains constant within errors during the short dips. However, during the long dips the line flux changes significantly and is positively correlated with the fluxes of the two hot components. These results suggest: (1) the temperature of the X-ray emitting region decreases with radius, (2) the Fe K α line emitting region is close to the hot continuum emitting region, and (3) the size of the Fe line emitting region is bigger than the size of the obscuring matters causing short dips but smaller than the sizes of those causing long dips.

Key words: stars: individual (Circinus X-1) – stars: neutron – X-rays: stars

1 INTRODUCTION

The X-ray light curves of some low mass X-ray binaries (LMXBs) contain dips, which usually occur near phase zero. In some cases, the dips may be due to the disk instability resulting in the rapid removal and replenishment of matter forming the inner part of an optically thick accretion disk (e.g., Belloni et al.

* E-mail: leiyj@mail.ihep.ac.cn

1997; Greiner et al. 1996). However, in most cases, the dips are suggested to be due to the absorption by the matter passing through the line of sight to the X-ray emitting region (e.g., White et al. 1995). The X-ray spectral evolution during the dips can provide us information about the geometry and physical conditions of these regions in LMXBs (e.g., Asai et al. 2000; Barnard et al. 2001).

The X-ray spectrum of a LMXB usually includes both the continuum and 6.4 keV Fe $K\alpha$ line emission components (e.g., Hirano et al. 1987; White et al. 1986). The continuum emission component is often described by the two different models developed in the 1980's: the Western model and Eastern model. The "Western model" suggests that Comptonization dominates the spectra, which has the form of a power law with high energy cut off corresponding to the energy limit of the Comptonizing electrons. However, for bright sources, an additive blackbody component representing the emission from the neutron star (NS) is needed (e.g., White et al. 1988). The "Eastern model" suggests that every observed spectrum contains two spectral components: multi-temperature disk blackbody emission from the inner disk and Comptonized emission provided by the seed photons of NS (e.g., Mitsuda et al. 1989). As declaimed, the physical conditions of the emission region can be described by the "Eastern model". For example, Done et al. (2002) assumed that there is an intrinsic low energy cut off in the spectrum at ~ 1 keV due to the lack of low energy seed photons, and the emission of NS is probably buried beneath an optically thick boundary layer. As a result, the boundary layer dominates the hard spectrum while the disk dominates the soft energies. More recently, a model was proposed and developed by Church et al. (Church & Bałucińska-Church 1995; Church et al. 1997; Bałucińska-Church et al. 1999), in which two continuum components exist in the dipping LMXBs: the simple blackbody emission from NS plus Comptonized emission from an extended accretion disk corona (ADC) above the accretion disk and a "progressive covering" description of absorption. In addition, this model ascribes the dips to the absorption of obscuring matter to the emission components. For example, in X1755-338 and X1624-490, the absorption to the blackbody component is primarily responsible for dipping (Church & Bałucińska-Church 1995, Church & Bałucińska-Church 1996), while in X1658-298 the absorption to the blackbody component is lower than that to the Comptonized component (Oosterbroek et al. 2001). In addition, for Cir X-1, Shirey et al. (1999) used a disk blackbody plus a blackbody and a "progressive covering" to fit the spectra during the dips; Ding et al. (2006a) fitted the dip spectra with the two blackbodies plus a "progressive covering" for a long dip of Cir X-1 (also see Brandt et al. 1996).

Fe $K\alpha$ line emission at 6.4 \sim 6.7 keV is a common feature in the spectra of LMXBs, but its origin is still in dispute. White et al. (1986) detected Fe $K\alpha$ emission line in five out of six LMXBs, and proposed that the emission line is produced by the recombination of Fe $XXVI$ in the inner ADC. Such a scenario was also suggested by Hirano et al. (1987). The Fe $K\alpha$ emission of dipping LMXBs is even more interesting since dips may provide new clues about the location of the line emitting region. Barnard et al. (2001) proposed that in XB 1323-619 the Fe line at ~ 6.4 keV originates probably in the ADC, while Smale et al. (1993) ascribed the Fe line emission to the reflection from the accretion disk itself for Cygnus X-2. Using *RXTE* data, Shirey et al. (1999) investigated the spectral evolution of Cir X-1 during dips and found that the Fe line flux is roughly constant during the dip transitions, suggesting the Fe $K\alpha$ emission to be produced in the scattering medium.

Dips occur frequently on the light curve of Cir X-1, providing a good opportunity to study statistically the structure of the X-ray emitting regions and

the location of Fe $K\alpha$ line. The spectral fits of the data of *ASCA*, *RXTE* and *BeppoSAX* during the dips are consistent with a partial covering model, in which the X-ray emission consists of a bright component undergoing varying absorbing matter and a faint component unaffected by the absorbing matter (e.g., Brandt et al 1996; Shirey et al. 1999; Iaria et al. 2001). The partial covering is a determinant of the behaviors observed from Cir X-1, and matter at the outer edge of the accretion disk, with an edge-on disk orientation, could explain the partial covering of the spectrum (Brandt et al. 1996). Ding et al. (2006a) studied a long dip of Cir X-1 and concluded that the covering matter exists from the surface of NS to the emitting region of iron line in the accretion disk. However, another standpoints also exist, for example, Díaz Trigo et al. (2006) showed that there is no need for partial covering to explain the spectral evolution during the dips with *XMM* data.

In those previous studies of the dips of Cir X-1, each paper is usually based on the spectral analysis of a particular dip. We therefore present herein a statistical study of the spectral evolution of Cir X-1 during various dips so as to better constrain the structure of the X-ray emitting regions. The paper is organized as follows: the observations, spectral models, and data analyses are described in Sect. 2, the results are shown in Sect. 3, the discussions are preseted in Sect. 4 and the summary is in Sect. 5.

2 OBSERVATIONS AND ANALYSIS

2.1 Observations and Light Curves

The Proportional Counter Array (PCA) of *RXTE* consists of 5 non-imaging, coaligned Xe multiwire proportional counter units (PCUs). It has a field of view of $1^\circ \times 1^\circ$ and a total collecting area of $\sim 6500 \text{ cm}^2$. We use five datasets collected by PCU0 and PCU2 when both of them are working, and both long (duration $\geq 10^4 \text{ s}$) and short (duration $\leq 10^4 \text{ s}$) dips are detected in these data (Table 1). Since we are interested in the spectral evolution during dips, we only study the dips with durations $\geq 10^2 \text{ s}$ so that each dip can be divided into a few segments and each segment contains enough counts for spectral analysis. Altogether we study the spectral properties of three long dips and two short dips that are divided each into 5-17 segments. Two typical light curves with the denoted segments are shown in Figs. 1 and 2.

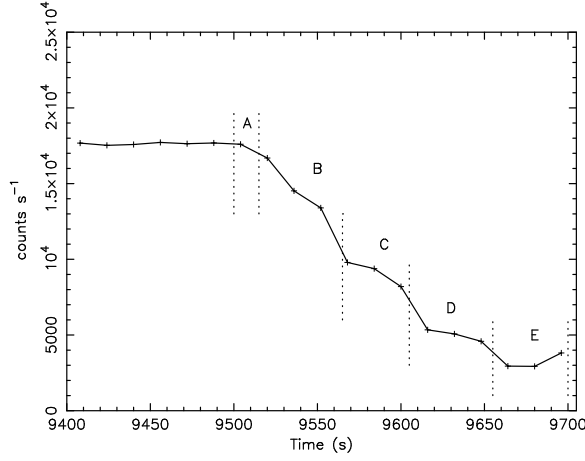
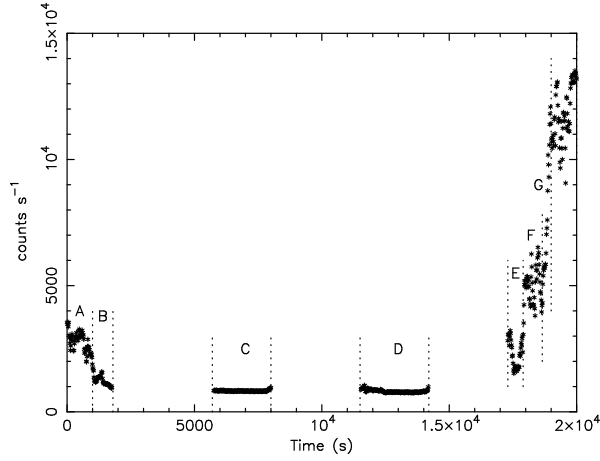
The data are reduced and analyzed using the *Ftools* software package version v5.2. We filter the data using the standard *RXTE* criteria, selecting time intervals for which parameters `ElevationAngles` $< 10^\circ$, `Time.Since.SAA` $\geq 30 \text{ min}$, `Pointing.Offsets` $< 0.02^\circ$, and the background electron rate `Electron2` < 0.1 . Events in the *RXTE* energy range $\sim 2.5\text{-}25 \text{ keV}$ are selected for the spectral analysis. PCA background subtraction is carried out using the latest versions of the appropriate background models, and a 1% systematic error is added to the spectra to account for calibration uncertainties. As usual, the spectral fitting software *XSPEC* is used.

2.2 Spectral Model

In the literature various spectral models have been used to fit the spectra of Cir X-1 during dips (e.g., Brandt et al. 1996; Shirey et al. 1999; Iaria et al. 2002; Ding et al. 2006a). Brandt et al. (1996) used a model containing two blackbody components and a partial covering. The partial covering can affect the hot component, two or none of them. Shirey et al. (1999) used a model which can be expressed

Table 1 Selected RXTE observations of Cir X-1

OBSID	Start Time	Stop Time	Exposure(s)
10122-01-04-00	96-9-20 07:47:01	96-9-20 12:30:13	16992
10122-01-04-02	96-9-21 04:40:02	96-9-21 11:01:13	22871
30080-01-01-000	98-03-03 16:42:14	98-03-03 23:22:07	23993
30081-06-01-000	98-10-05 00:07:41	98-10-05 08:01:07	28406
30081-06-01-01	98-10-04 22:31:54	98-10-04 23:36:14	3860
60024-01-01-00	01-02-28 06:54:03	01-02-28 09:10:15	8172
60024-01-01-01	01-02-28 03:40:03	01-02-28 05:59:15	8352
60024-01-01-02	01-02-28 02:00:41	01-02-28 02:48:15	2854
60024-02-01-03	01-02-28 09:41:03	01-02-28 10:10:15	1752

**Fig. 1** Typical light curve (16 s bins) of short ($< 10^4$ s) dip during dip and dip transition from PCA observations of Cir X-1 (OBSID:30080). For clarity, the errors are not plotted.**Fig. 2** Typical light curve (16 s bins) of long ($> 10^4$ s) dip during dip and dip transition from PCA observations of Cir X-1 (OBSID:30081).

as: $F = [\exp(-\sigma_{ph} N_H^{(1)}) \exp(-\sigma_{Th} N_H^{(1)}) + \exp(-\sigma_{ph} N_H^{(2)}) f] M$, where F is the observed flux, σ_{ph} and σ_{Th} are the photoelectric and Thomson cross sections, $N_H^{(1)}$ and $N_H^{(2)}$ are the effective absorption hydrogen column densities to the bright and faint components, respectively, f is the ratio of the unabsorbed flux of the faint component to the unabsorbed flux of the bright component, and M is the disk blackbody plus blackbody model. Ding et al. (2006a) fitted the dip spectra with the “Eastern” model and a modified “Western” model.

However, we find that all these above mentioned spectral models are improper to reveal the physical conditions of the dips. In Brandt et al. (1996) and Ding et al. (2006a), one of the fitted temperatures changes greatly within a dip. For an example, the temperature of the disk-blackbody component changes suddenly from ~ 0.6 keV to ~ 1.2 keV when its detected fluxes evolves from the dip bottom to the transition state. Such temperature changes seem unlikely if the dips are mainly due to the obscuration as widely accepted, because the obscuring matter can not change the physical state of the emission region. In the model of Shirey et al. (1999), the residual flux at the bottom of the dips is a fraction of the total emission. However, the hardness-intensity diagram (Fig. 3 in their paper and this paper) shows that the detected spectrum of Cir X-1 at the lowest flux level is even softer than that of its out-of-dip. This means that the residual emission spectrum at dip bottom is intrinsically softer than that nondip spectrum, i.e., it is improper to assume that the residual emission is simply a small fraction of the total emission.

The soft spectrum at the bottom of the dip and the sudden temperature increase of the disk-blackbody component (Ding et al. 2006a) when Cir X-1 moves to the transition state, imply that there exists a weak and soft component which is not affected by the obscuring matter. When there is no dip or in the transition state, the usually called “NS blackbody emission and disk-blackbody emission” dominate, and so the weak component is difficult to be noted. When most of the “NS blackbody emission and disk-blackbody emission” are obscured when Cir X-1 is at the bottom of the dips, the contribution of the weak and soft component to the total flux becomes significant or even dominant, and so the detected spectrum at the dip bottom is softer than the out-of-dip spectrum. Such a weak and soft component is also noted by Ding et al. (2006a) but they do not consider it further in the spectral fitting process.

Taking the above facts into account, we use in this paper a spectral model containing three blackbody components and a Gaussian at the energy of Fe K α line. The first two blackbody components with partial covering are similar to those models in Brandt et al. (1996), Shirey et al. (1999) and Ding et al. (2006a), while the additional third component represents the weak and soft emission that are free of partial covering absorption. The expression of our model is: $F = wabs[pcfabs * cabs(bbodyrad(1) + bbodyrad(2) + gaussian) + bbodyrad(3)]$, where $wabs$ represents the photoelectric absorption of the interstellar medium (ISM), $pcfabs$ corresponds to the partial covering photoelectric absorption, $cabs$ accounts for the Compton scattering of the partial covering matter, $bbodyrad(1)$ and $bbodyrad(2)$ represent the continuum emission which is affected by the partial covering, $bbodyrad(3)$ is responsible for the soft faint emission component, and $gaussian$ accounts for the Fe K α line emission. As shown later, the fitted parameters by this model are much more reasonable than those in Brandt et al. (1996), Shirey et al. (1999) and Ding et al. (2006a).

In the spectral fitting, the column density of $wabs$ is fixed as $1.8 \times 10^{22} \text{ cm}^{-2}$ as determined in the previous work (e.g., Brandt et al. 1996; Iaria et al. 2001), and the column densities of $pcfabs$ and $cabs$ are forced to be identical (Shirey et al. 1999). As shown by the following fitting results (Figs. 4-9, Tables 2-3), such

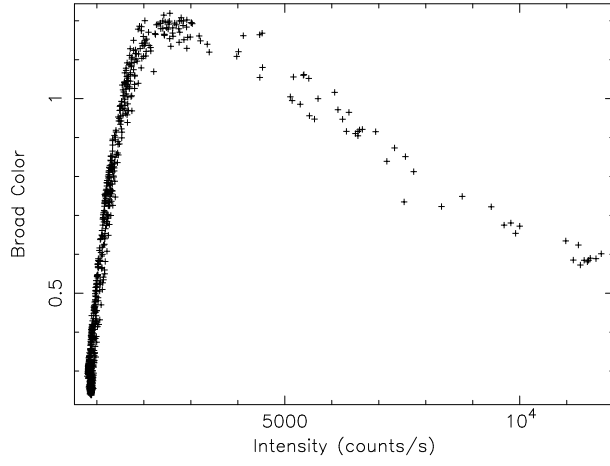


Fig. 3 Hardness-intensity diagram for data in Fig. 2, intensity is $I(2.0-18 \text{ keV})$, the hardness ratio is defined as : $I(6.3-18 \text{ keV})/I(2.0-6.3 \text{ keV})$. Each point represents 16 s of background-subtracted data from all five PCA detectors (also see, Shirey et al. 1999).

a model gives statistically acceptable fits to both the dip and nondip spectra, and the obtained parameters look physically reasonable.

3 RESULT

The spectra of all the segments have been fitted with the model described in Sect. 2. Tables 2 and 3 list the spectral fitting results for segments in OBSIDs 30080 and 30081. In the following we will present our results in various aspects.

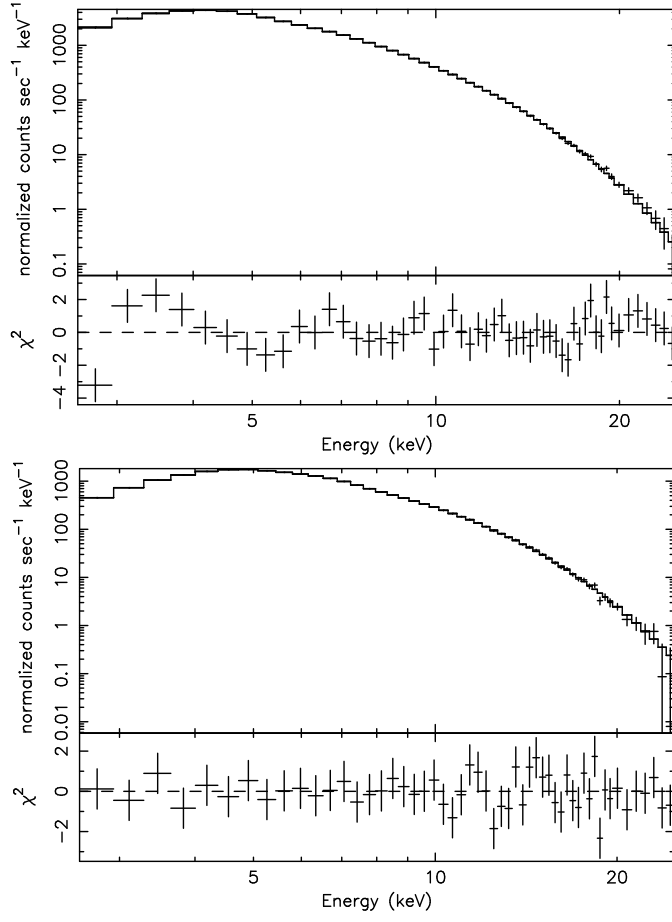


Fig. 4 Top: Typical spectral fit for the dip spectra (spectrum C of OBSID 30080 in Table 2). Bottom: Typical spectral fit for the nondip spectra (nondip data of OBSID 30080), with χ^2 values of 55.4 for 54 degrees of freedom.

Table 2 The Fitted Parameters for Spectra from the OBSID 30080 dip

Fit Parameters	A	B	C	D	E
N_H^a	1.8(fixed)	1.8(fixed)	1.8(fixed)	1.8(fixed)	1.8(fixed)
N_H^b	$0.0^{+6.3}_{-0.0}$	$2.4^{+0.6}_{-0.3}$	16^{+3}_{-8}	34^{+6}_{-5}	38^{+13}_{-21}
Percentage ^c	$4.85^{+95.15}_{-4.85}$	95.2(fixed)	$75.0^{+24.4}_{-4.0}$	$89.9^{+2.8}_{-2.9}$	$81.0^{+4.2}_{-5.1}$
kT_1^d (keV)	$1.85^{+0.04}_{-0.04}$	$1.87^{+0.05}_{-0.05}$	$1.91^{+0.07}_{-0.08}$	$1.97^{+0.10}_{-0.08}$	$1.89^{+0.08}_{-0.08}$
A_1^e	107^{+9}_{-16}	$93.7^{+22.3}_{-8.8}$	$80.1^{+21.4}_{-22.7}$	$61.9^{+23.3}_{-10.7}$	$81.7^{+36.3}_{-23.2}$
$flux_1^m$	$1.11^{+0.22}_{-0.16}$	$0.85^{+0.22}_{-0.15}$	$0.49^{+0.21}_{-0.13}$	$0.21^{+23.3}_{-10.7}$	$0.26^{+0.12}_{-0.08}$
E_{line}^f (keV)	6.60(fixed)	$6.56^{+0.33}_{-0.28}$	$6.48^{+0.47}_{-0.49}$	6.60(fixed)	$6.64^{+0.34}_{-0.26}$
σ^g (keV)	0.5(fixed)	0.5(fixed)	$0.58^{+0.70}_{-0.58}$	$0.36^{+0.21}_{-0.36}$	$0.22^{+0.40}_{-0.22}$
$flux^h$	$12.93^{+5.76}_{-8.71}$	$16.98^{+4.95}_{-9.21}$	$22.33^{+47.80}_{-14.39}$	$14.14^{+8.10}_{-2.95}$	$14.65^{+16.54}_{-4.29}$
kT_2^i (keV)	$1.00^{+0.03}_{-0.04}$	$1.03^{+0.01}_{-0.04}$	$1.06^{+0.05}_{-0.12}$	$1.12^{+0.06}_{-0.05}$	$1.08^{+0.06}_{-0.04}$
A_2^j	$3.36^{+0.43}_{-0.33} \times 10^3$	$2.74^{+0.25}_{-0.30} \times 10^3$	$2.19^{+0.58}_{-0.41} \times 10^3$	$1.69^{+0.42}_{-0.21} \times 10^3$	$1.65^{+0.95}_{-0.81} \times 10^3$
$flux_2^n$	$3.92^{+0.43}_{-0.33}$	$2.65^{+0.48}_{-0.28}$	$1.35^{+0.50}_{-0.51}$	$0.57^{+0.17}_{-0.14}$	$0.57^{+0.34}_{-0.28}$
kT_3^k (keV)	0.50(fixed)	0.50(fixed)	0.50(fixed)	$0.49^{+0.02}_{-0.02}$	0.50(fixed)
A_3^l	$4.60^{+8.38}_{-4.38} \times 10^3$	$0.0^{+2.93}_{-0.0} \times 10^3$	$0.02^{+6.47}_{-0.02} \times 10^3$	$8.45^{+7.08}_{-3.83} \times 10^3$	$5.32^{+3.87}_{-2.16} \times 10^3$
$flux_3^p$	$0.19^{+0.35}_{-0.18}$	$0.0^{+0.12}_{-0.0}$	$0.0^{+0.28}_{-0.0}$	$0.31^{+0.26}_{-0.14}$	$0.22^{+0.13}_{-0.07}$
χ^2 (dof) ^p	68.63(46)	42.82(46)	35.51(44)	30.46(45)	24.04(44)
χ_ν^{2q}	1.49	0.93	0.81	0.68	0.55

NOTE Model of wabs[pcfabs*cabs(bbodyrad(1)+gaussian+bbodyrad(2))]+wabs*bbodyrad(3) is used. Uncertainties are given at 90% confidence level.

^a Interstellar column density, in units of 10^{22} cm^{-2}

^b Partial covering column density, in units of 10^{22} cm^{-2}

^c Partial covering percentage

^d The temperature of blackbody(1)

^e The normalization of blackbody(1)

^m The flux of blackbody(1) in the 2.0-10.0 keV energy range and in units of photons $\text{cm}^{-2} \text{ s}^{-1}$

^f Gaussian line energy

^g Gaussian width

^h Flux of the gaussian line, in units of $10^{-3} \text{ photons cm}^{-2} \text{ s}^{-1}$

ⁱ The temperature of blackbody(2)

^j The normalization of blackbody(2)

ⁿ The flux of blackbody(2) in the 2.0-10.0 keV energy range and in units of photons $\text{cm}^{-2} \text{ s}^{-1}$

^k The temperature of blackbody(3)

^l The normalization of blackbody(3)

^p The flux of blackbody(3) in the 2.0-10.0 keV energy range and in units of photons $\text{cm}^{-2} \text{ s}^{-1}$

^p χ^2 (dof): χ^2 : Chi-Squared; dof: degrees of freedom

^q χ_ν^2 : reduced chi-squared: χ^2/dof

Table 3 The Fitted Parameters for Spectra of the OBSID 30081 dip

Fit Parameters	A	B	C	D	E	F	G
N_H^a	1.8(fixed)	1.8(fixed)	1.8(fixed)	1.8(fixed)	1.8(fixed)	1.8(fixed)	1.8(fixed)
N_H^b	43^{+3}_{-4}	81^{+29}_{-42}	325^{+39}_{-53}	247^{+29}_{-40}	44^{+10}_{-8}	23^{+5}_{-4}	13^{+5}_{-8}
Percentage ^c	$98.1^{+1.9}_{-9.2}$	$82.9^{+7.6}_{-7.1}$	$89.6^{+2.8}_{-5.3}$	$90.8^{+2.8}_{-5.4}$	$98.0^{+2.0}_{-7.3}$	95.2(fixed)	$55.1^{+44.9}_{-5.5}$
kT_1^d (keV)	$2.14^{+0.04}_{-0.03}$	$2.11^{+0.08}_{-0.07}$	2.20(fixed)	$2.25^{+0.42}_{-0.19}$	$2.11^{+0.05}_{-0.05}$	$2.10^{+0.04}_{-0.04}$	$2.05^{+0.03}_{-0.04}$
A_1^e	$37.3^{+5.0}_{-5.1}$	$31.0^{+45.4}_{-13.9}$	$36.9^{+8.7}_{-5.6}$	$33.5^{+29.9}_{-24.8}$	$37.7^{+9.7}_{-7.4}$	$41.6^{+6.8}_{-5.8}$	$50.0^{+4.2}_{-9.3}$
$flux_1^m$	$0.11^{+0.02}_{-0.02}$	$0.06^{+0.09}_{-0.03}$	$0.00^{+0.00}_{-0.00}$	$0.01^{+0.01}_{-0.01}$	$0.10^{+0.32}_{-0.02}$	$0.23^{+0.04}_{-0.03}$	$0.47^{+0.04}_{-0.09}$
E_{line}^f (keV)	6.60(fixed)	$6.63^{+0.11}_{-0.13}$	$6.56^{+0.06}_{-0.04}$	$6.55^{+0.05}_{-0.05}$	$6.64^{+0.32}_{-0.20}$	$6.65^{+0.27}_{-0.24}$	$6.42^{+0.32}_{-0.40}$
σ^g (keV)	0.50(fixed)	$0.38^{+0.18}_{-0.13}$	$0.20^{+0.12}_{-0.20}$	$0.26^{+0.09}_{-0.15}$	$0.45^{+0.24}_{-0.31}$	$0.39^{+0.28}_{-0.39}$	$0.54^{+0.30}_{-0.43}$
$flux^h$	$7.36^{+2.88}_{-3.40}$	$8.17^{+4.86}_{-2.60}$	$4.90^{+2.54}_{-2.81}$	$5.64^{+3.94}_{-2.77}$	$14.63^{+3.74}_{-6.14}$	$17.21^{+12.25}_{-7.34}$	$29.31^{+16.96}_{-13.68}$
kT_2^i (keV)	$1.19^{+0.03}_{-0.03}$	$0.84^{+0.13}_{-0.22}$	$1.27^{+0.07}_{-0.07}$	$1.29^{+0.13}_{-0.08}$	$1.21^{+0.06}_{-0.05}$	$1.17^{+0.03}_{-0.03}$	$1.12^{+0.02}_{-0.03}$
A_2^j	$0.89^{+0.19}_{-0.15} \times 10^3$	$2.13^{+4.86}_{-1.35} \times 10^3$	$4.11^{+3.31}_{-1.73} \times 10^3$	$2.15^{+1.39}_{-1.09} \times 10^3$	$0.68^{+0.50}_{-0.17} \times 10^3$	$1.16^{+0.30}_{-0.26} \times 10^3$	$1.33^{+0.34}_{-0.46} \times 10^3$
$flux_2^j$ (keV)	$0.23^{+0.05}_{-0.04}$	$0.12^{+0.26}_{-0.07}$	$0.09^{+0.07}_{-0.05}$	$0.09^{+0.05}_{-0.04}$	$0.17^{+0.13}_{-0.08}$	$0.61^{+0.16}_{-0.16}$	$1.40^{+0.35}_{-0.47}$
kT_3^k (keV)	$0.58^{+0.02}_{-0.02}$	$0.54^{+0.07}_{-0.07}$	$0.53^{+0.01}_{-0.02}$	$0.51^{+0.03}_{-0.01}$	$0.54^{+0.02}_{-0.02}$	$0.48^{+0.11}_{-0.09}$	0.50(fixed)
A_3^l	$3.61^{+0.70}_{-0.62} \times 10^3$	$4.11^{+2.51}_{-1.57} \times 10^3$	$4.71^{+1.06}_{-0.71} \times 10^3$	$5.33^{+0.97}_{-0.54} \times 10^3$	$4.32^{+1.23}_{-0.91} \times 10^3$	$6.75^{+18.16}_{-4.44} \times 10^3$	$0.0^{+6.85}_{-0.0} \times 10^3$
$flux_3^p$	$0.35^{+0.06}_{-0.06}$	$0.26^{+0.15}_{-0.08}$	$0.28^{+0.03}_{-0.04}$	$0.26^{+0.05}_{-0.05}$	$0.28^{+0.08}_{-0.06}$	$0.22^{+0.60}_{-0.16}$	$0.0^{+0.23}_{-0.0}$
χ^2 (dof) ^p	17.68(45)	20.32(43)	23.32(44)	21.17(43)	15.54(43)	18.28(44)	18.45(44)
χ_ν^{2q}	0.39	0.47	0.53	0.49	0.36	0.42	0.42

NOTE Model of wabs[pcfabs*cabs(bbodyrad(1)+gaussian+bbodyrad(2))]+wabs*bbodyrad(3) is used. Uncertainties are given at 90% confidence level for the derived parameters of the model applied.

^aInterstellar column density, in units of 10^{22} cm^{-2}

^bPartial covering column density, in units of 10^{22} cm^{-2}

^cPartial covering percentage

^dThe temperature of blackbody(1)

^eThe normalization of blackbody(1)

^mThe flux of blackbody(1) in the 2.0-10.0 keV energy range and in units of photons $\text{cm}^{-2} \text{ s}^{-1}$

^fGaussian line energy

^gGaussian width

^hFlux of the gaussian line, in units of $10^{-3} \text{ photons cm}^{-2} \text{ s}^{-1}$

ⁱThe temperature of blackbody(2)

^jThe normalization of blackbody(2)

ⁿThe flux of blackbody(2) in the 2.0-10.0 keV energy range and in units of photons $\text{cm}^{-2} \text{ s}^{-1}$

^kThe temperature of blackbody(3)

^lThe normalization of blackbody(3)

^pThe flux of blackbody(3) in the 2.0-10.0 keV energy range and in units of photons $\text{cm}^{-2} \text{ s}^{-1}$

^p χ^2 (dof): χ^2 : Chi-Squared; dof: degrees of freedom

^q χ_ν^2 : reduced chi-squared: χ^2/dof

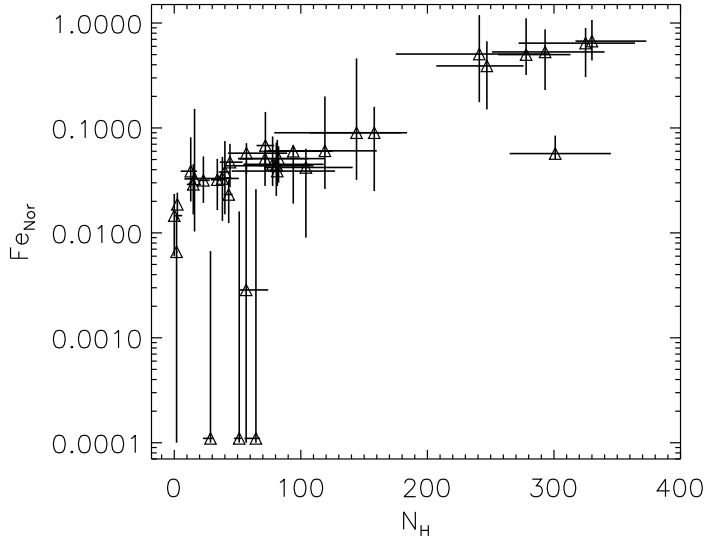


Fig. 5 The normalization of Fe line is plotted against N_H (in units of 10^{22} cm^{-2}), and an obvious correlation can be found.

3.1 Partial covering column density and the correlations with other parameters

Brandt et al. (1996) used a partial covering model to fit the spectra before and after the dip transition of Cir X-1, and found a strong Fe $K\alpha$ edge in the low-state spectra, which indicates that the obscuring matter has a very high column density, i.e. $N_H > 10^{24} \text{ cm}^{-2}$. Shirey et al. (1999) obtained a similar result. Our results show that the hydrogen column density of partial covering absorption is between 10^{22} cm^{-2} and $3.3 \times 10^{24} \text{ cm}^{-2}$ (e.g., Fig. 5). The large variation of column density could be due to the partial covering and/or the inhomogeneity of the covering matter.

Figures 5 and 6 show relations of the normalizations of the Fe $K\alpha$, blackbody(1) and blackbody(2) versus the partial covering absorption column density. Obviously, the normalization of Fe $K\alpha$ line has a positive correlation with N_H , while the correlations are weak for the normalizations of blackbody(1) and blackbody(2). Since in the spectral fitting, the absorption column density and normalization are usually coupled with each other, in order to check whether the correlation between the Fe $K\alpha$ strength and the absorption column density is real or not, we derive the normalization ratios of the Fe $K\alpha$ normalization to the normalizations of blackbody(1) and blackbody(2). As shown in Figs. 7 and 8, such coupling-free ratios are also correlated with the absorption column density, indicating that the origin of the Fe emission line is related to the obscuration matter.

3.2 Temperatures and Sizes of emission regions

For every dip, the temperature of blackbody(1) is about 2 keV and that of blackbody(2) is about 1 keV, which is consistent with the results of Shirey et al. (1999) with *RXTE*. The temperature of blackbody(3), unaffected by the partial cover-

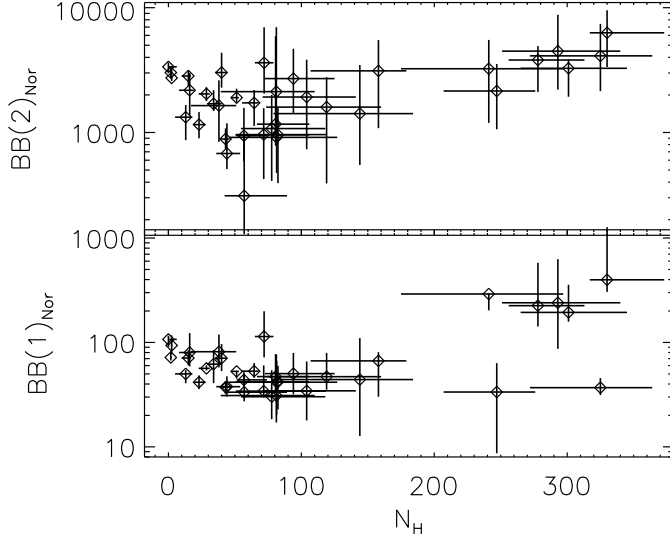


Fig. 6 The normalizations of blackbody(1) (bottom) and blackbody(2) (top) are plotted against N_H , and both show the correlations.

ing, is about 0.5~0.6 keV, which is consistent with the result of Brandt et al. (1996) with ASCA. The almost constant values of the temperature also show that the selecting of a three-blackbody-component spectral model is proper.

The distance to Cir X-1 is about 6-10 kpc (e.g., Stewart et al. 1991; Goss & Mebold 1977), so we adopt a value of 8 kpc in converting the blackbody normalization to radius. Hence, the obtained radii of blackbody(1) (blackbody(2)) are mostly in the range of 4-7 km (16-30 km). As for the blackbody(3), usually, its radii lie in the range of 30-50 km. Since the typical radius of a NS is 10 km, blackbody(1) may come from hot regions near/on the NS surface, while blackbody(2) and blackbody(3) are perhaps from the inner and outer disk respectively.

3.3 Flux and Flux correlations

In Fig. 9 we plot the relations between the fluxes of blackbody(1), blackbody(2) and blackbody(3). A strong correlation between the fluxes of blackbody(1) and blackbody(2) is found, with a correlation coefficient $0.98^{+0.02}_{-0.04}$. However, further investigations have not shown any sign of clear correlations between the flux of blackbody(3) and that of blackbody(1) or blackbody(2).

We now show that the linear correlation between the fluxes of blackbody(1) and blackbody(2) is intrinsic other than a false appearance of the spectral fitting. In the spectral fitting, blackbody(1) and blackbody(2) are all coupled with the partial covering. When the partial covering column density (and/or covering fraction) is somehow overestimated, the normalizations of the two components will be in turn higher than the real values, and vice versa. Then the two normalizations will show an artificial positive correlation. However, the fluxes plotted in Fig. 9 are the absorbed ones (corresponding to the observed fluxes), in which the model coupling effect is eliminated. Therefore, the linear correlations shown in Fig. 9 is reliable.

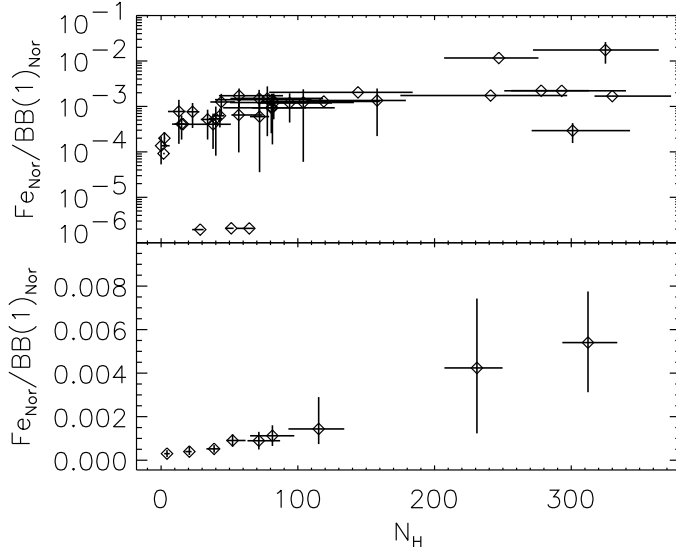


Fig. 7 Ratio of the normalization of Fe line to that of blackbody(1) is plotted against N_H . The bottom panel is a four-point binned plot of the top one, a positive correlation can be seen.

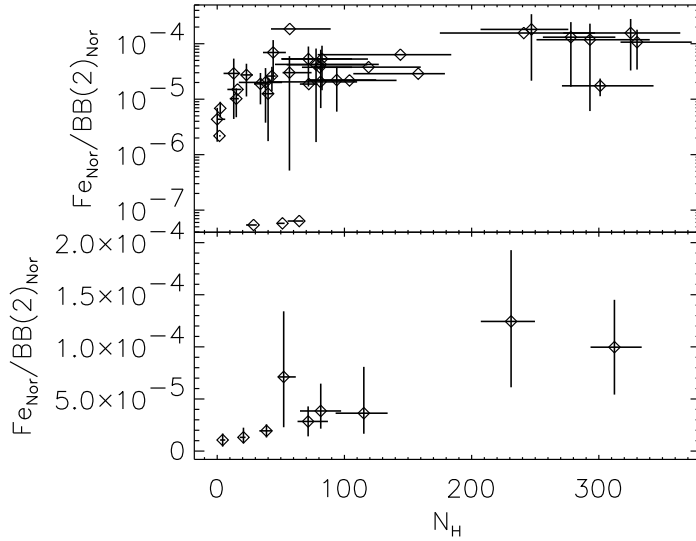


Fig. 8 Similar to Fig. 7, but blackbody(2) is substituted.

The flux correlation between blackbody(1) and blackbody(2) implies that these two components are usually obscured simultaneously. So their emission regions are probably very close to each other. This is well consistent with the conclusions we drew from the equivalent emitting radii in the previous section.

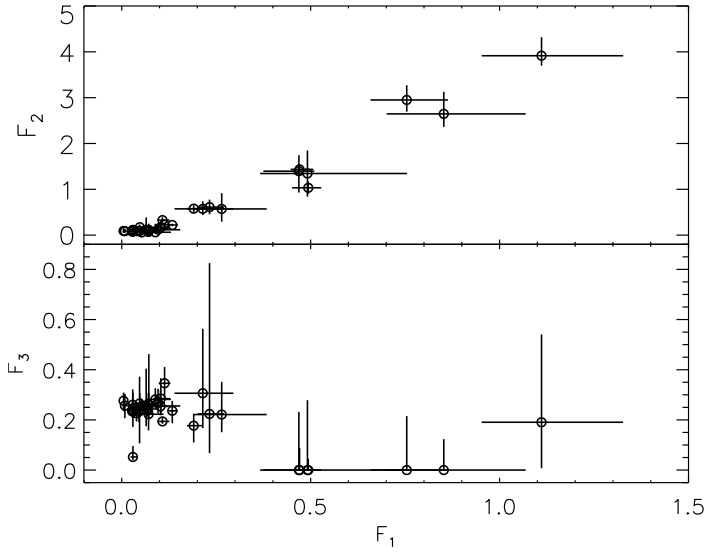


Fig.9 The flux (in units of $\text{photons cm}^{-2} \text{s}^{-1}$) of blackbody(1) plotted against that of blackbody(2) (top panel) and blackbody(3) (bottom panel). The top panel clearly shows a linear correlation, whereas no significant relationship has been revealed in the bottom panel.

3.4 Fe line flux and its correlations with continuum components

Figure 10 plots the Fe line fluxes versus the fluxes of the continuum components. It is found that the flux of the Fe line has a trend to increase along with the fluxes of blackbody(1) and blackbody(2), while no clear correlation exists between the Fe line flux and that of blackbody(3). Since the flux changes for both the line and continuum emission are mainly due to the obscuration of partial covering matters, this correlation suggests that the Fe line emission originates close to the hot regions that emit blackbody(1) and blackbody(2).

We further divide the dips into long and short dips, and for each category, we investigate the above correlations. As plotted in Fig. 11, for long dips, the flux of Fe line has now even better correlations with those of the blackbody(1) and blackbody(2) than the correlations for all the dips. However, for short dips, such correlations do not exist anymore (see Fig. 12), which is consistent with the results of Shirey et al. (1999). Similar to that for all the dips, correlations between the flux of the Fe line and that of blackbody(3) are not detected either for long dips or for short dips. These results tell us that the emitting region of the Fe line is smaller than the obscuration matters of long dips but bigger than those of the short dips.

4 DISCUSSION

The binary system of Cir X-1 has a highly eccentric orbit. Possibly, the NS may be occulted by the outer layers of its companion atmosphere when the star moves close to the periastron. The high eccentricity of the orbit might produce large tidal interactions at this phase, in turn, which perhaps expand and/or deform the accretion stream, or maybe form a bulge in the outer accretion disk. The excess of

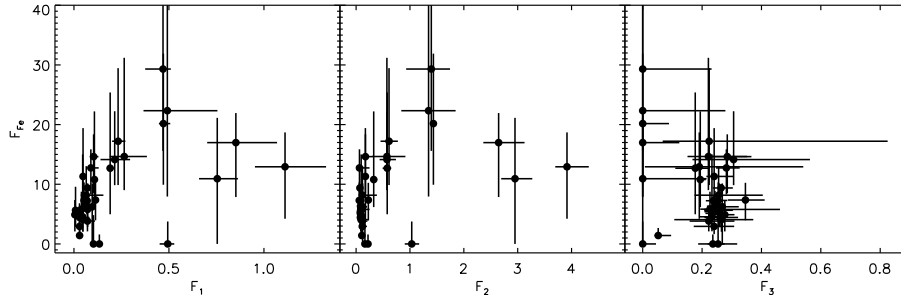


Fig. 10 Fe line flux (in units of 10^{-3} photons $\text{cm}^{-2} \text{s}^{-1}$) plotted as a function of the flux of blackbody(1) (left), blackbody(2) (middle) and blackbody(3) (right), for all chosen dips (10122-dip1, 30081, 60024, 10122-dip2, 30080).

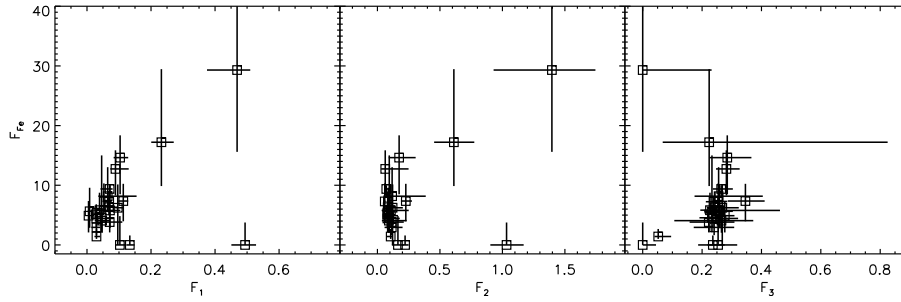


Fig. 11 Similar to Fig. 10, but for the long dips (10122-dip1, 30081, 60024). The left (middle) panel shows a correlation, and no significant relationship has been noticed in the right one.

these matters may influence on the observed emission of X-ray source, producing a partial covering of the energy spectrum of the source (e.g., Inoue 1989; Iaria et al. 2001).

The Fe $K\alpha$ line emission at 6.4~6.7 keV is a common feature in LMXBs, and its origin has been an interesting topic. Generally, there are four possible sites for the Fe $K\alpha$ emissions: the accretion disk, ADC, the source itself, or the scattering medium (e.g., Smale et al. 1993; Shirey et al. 1999; Asai et al. 2000). The observed strong broad line at 6.4~6.7 keV is generally interpreted as arising from the ADC and illuminated outer disk (e.g., White et al. 1985; Hirano et al. 1987; Asai et al. 2000), but it is difficult to obtain both the observed line intensity and width from such a corona.

For Cir X-1, the results of Shirey et al. (1999) show that the Fe $K\alpha$ line flux is constant and associated with the faint component during short dips, implying that the Fe $K\alpha$ comes from the scattering medium far away from the central region. After investigating the long dip of Cir X-1, Ding et al. (2006a,b) propose that Fe line emission is from the disk. Our results show that the flux of iron line emission changes obviously during the long dips (see OBSID 30081 of Table 3) and is positively correlated with the fluxes of blackbody(1) and blackbody(2).

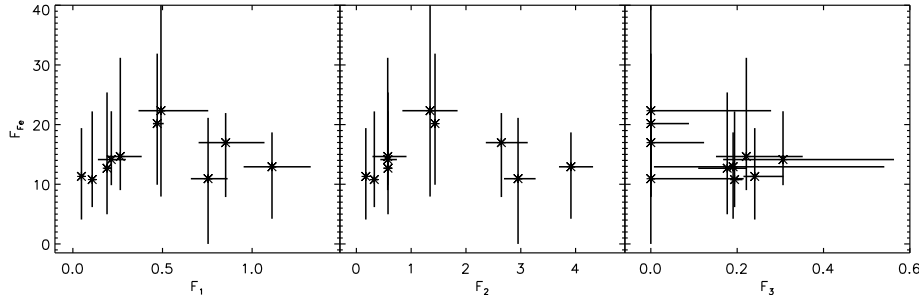


Fig. 12 Similar to Fig. 10, but for the short dips (10122-dip2, 30080). The Fe line flux is almost unchanged, within the errors, regarding to all continuum spectrum fluxes.

This token implies that the line could not be associated with the soft component unaffected by the partial covering, and instead, it is affected by the partial covering and could come from the region close to the central object.

For short dips, our result shows that the flux of the Fe emission line is almost constant. There are two possible interpretations for this constant Fe line emission flux: (1) for the short dip the obscuring matter could be of a small size, and (2) the obscuring matter lies inner than the Fe line emission materials on the accretion disk. On the other hand, according to the fact that the normalization of the Fe line is positively correlated with N_H (see Fig. 5), we also considered that the Fe line could come from the accreting matter, which suggests that the Fe line strength is related to mass accretion rate. Dong et al. (2004) showed that the equivalent width of the Fe line was associated with column density, implying that the line could come from the cold matter invoked in an absorbed model for active galactic nuclei (AGNs) NGC 2110 and NGC 7582. However, Asai et al. (2000) analyzed the Fe $K\alpha$ emission lines in the spectra of 20 LMXBs using *ASCA* data, and found that the centroid energies of the Fe lines are almost independent of the source luminosity, and the detected equivalent width of the line also does not show a clear correlation with the source categories. Although the physical parameters of determining the distinction of these categories has not been figured out, the inclination angle, mass accretion rate, and the stellar magnetic field are the most relevant quantities. Thus, Asai et al. (2000) proposed that these parameters may not play a key role in determining the Fe line strength. Unlike the conclusions of Asai et al. (2000), our results favor that the Fe emission line might be correlated with the accreting matter and come from the inner accretion disk.

Nevertheless, we also noticed some discussions about the origin of the Fe emission line of other objects. For some black hole candidates, there is evidence that the observed Fe $K\alpha$ line originates in the innermost part of the accretion disk, close to the black hole (e.g., Fabian et al. 1989; Cui et al. 1998; Zychi et al. 1999). In addition, for AGNs, the higher resolution spectra available with the *ASCA* appear to indicate that the line profiles are broad and asymmetrically skewed to lower energies, which is interpreted as evidence that the majority of the line emission origin from the inner accretion disk around the massive black hole (Nandra et al. 1997; Reynolds & Begelman 1997). Nandra et al. (2000) presented a spectral analysis of the Seyfert 1 galaxy NGC 7469 with *RXTE*, and found a significant correlation between the 2-10 keV flux and the 6.4 keV Fe $K\alpha$

line, suggesting that the line emission comes from very nearby central regions. Our results imply that the Fe line emission region on the accretion disk of an X-ray binary may be located at the same relative region as on the disk of an AGN.

5 CONCLUSION

In this paper, we analyzed the X-ray dip spectra of Cir X-1. The spectra can be well fitted with two blackbody components with the partial covering plus a third blackbody which is unaffected by partial covering. According to the spectral fitting results, the equivalent blackbody emission radii of the first ($T \sim 2$ keV), second ($T \sim 1$ keV) and third ($T = 0.5 \sim 0.6$ keV) component are, respectively, 4-7 km, 16-30 km, 30-50 km. The fluxes of the first and second components are closely correlated, indicating that they represent emission from the inner regions. The emitting region of the coolest (3rd) component might come from the outer accretion disk.

A 6.4-6.7 keV Fe emission line was detected in the dip spectra. During the long dips, the Fe line flux and fluxes of the first and second components are correlated, and there is no significant correlation between the Fe line flux and the flux of the third component, which suggests the Fe emission line comes from the region very close to the central object and is affected by the covering matter. During the short dip, the Fe line flux is almost constant within the errors for all continuum spectra fluxes, which might be due to the fact that the line emission region lie in the outer of the obscuring matter or the size of the obscuring matter is much smaller than that of the Fe line emitting region.

Acknowledgements We would like to thank T.P. Li and S. N. Zhang for useful discussions. This research has made use of data obtained through the High Energy Astrophysics Science Archive Research Center Online Service, provided by the NASA/Goddard Space Flight Center. We acknowledge the *RXTE* data teams at NASA/GSFC for their help. This work is subsidized by the Special Funds for Major State Basic Research Projects and by the National Natural Science Foundation of China. We are very grateful for the critic comments from the anonymous referee that greatly improve the quality of the paper.

References

- Asai K., Dotani T., Nagase F. et al. 2000, *ApJS*, 131, 571
- Barnard R., Balucińska-Church M., Smale A. P. et al. 2001, *A&A*, 380, 494
- Balucińska-Church M., Church M. J., Oosterbroek T. et al., 1999, *A&A*, 349, 495
- Belloni T., Mendez M., King A. R. et al., 1997, *ApJ*, 479, L145
- Brandt W. N., Fabian A. C., Dotani T. et al., 1996, *MNRAS*, 283, 1071
- Church M. J., Balucinska-Church M., 1995, *A&A*, 300, 441
- Church M. J., Balucińska-Church M., 1996, *Memorie della Societa Astronomica Italiana*, 67, 395
- Church M. J., Dotani T., Balucinska-Church M. et al., 1997, *ApJ*, 491, 388
- Cui W., Ebisawa K., Dotani T. et al., 1998, *ApJ*, 493, L75
- Díaz Trigo M., Parmar A. N., Boirin L. et al., 2006, *A&A*, 445, 179
- Ding G.Q., Qu J.L., Li T.P., 2006a, *AJ*, 131, 1693
- Ding G. Q., Zhang S. N., Li T. P. et al., 2006b, *ApJ*, 645, 576
- Done C., Życki P. T., Smith D. A., 2002, *MNRAS*, 331, 453

- Dong H., Xue S.J., Li C. et al., 2004, *Chin. J. Astron. Astrophys. (ChJAA)*, 4, 427
- Fabian A. C., Rees M. J., Stella L. et al., 1989, *MNRAS*, 238, 729
- Goss W. M., Mebold U., 1977, *MNRAS*, 181, 255
- Greiner J., Morgan E. H., Remillard R. A., 1996, *ApJ*, 473, L107
- Hirano T., Hayakawa S., Nagase F. et al., 1987, *PASJ*, 39, 619
- Iaria R., Di Salvo T., Burderi L. et al., 2001, *ApJ*, 561, 321
- Iaria R., Di Salvo T., Robba N. R. et al., 2002, *ApJ*, 567, 503
- Inoue H., 1989, *ESA SP-296: Two Topics in X-Ray Astronomy*, Vol. 1: X Ray Binaries. Vol. 2: AGN and the X Ray Background, 109
- Mitsuda K., Inoue H., Nakamura N., Tanaka Y., 1989, *PASJ*, 41, 97
- Nandra K., Le T., George I. M. et al., 2000, *ApJ*, 544, 734
- Nandra K., Mushotzky R. F., Yaqoob T. et al., 1997, *MNRAS*, 284, L7
- Oosterbroek T., Parmar A. N., Sidoli L. et al., 2001, *A&A*, 376, 532
- Reynolds C. S., Begelman M. C., 1997, *ApJ*, 488, 109
- Shirey R. E., Levine A. M., Bradt H. V., 1999, *ApJ*, 524, 1048
- Smale A. P. et al., 1993, *ApJ*, 410, 796
- Stewart R. T., Nelson G. J., Penninx W. et al., 1991, *MNRAS*, 253, 212
- White N., Nagase F., Parmar A. N., 1995, in *X-ray Binaries*, ed. W. G. H. Lewin J. van Paradijs, E. P. J. van den Heuvel (Cambridge: Cambridge Univ. Press), 1
- White N. E., Peacock A., Hasinger G. et al., 1986, *MNRAS*, 218, 129
- White N. E., Peacock A., Taylor B. G., 1985, *ApJ*, 296, 475
- White N. E., Stella L., Parmar A. N., 1988, *ApJ*, 324, 363
- Zycki P. T., Done C., Smith D. A., 1999, *MNRAS*, 305, 231